SANDIA REPORT

SAND89—0750 • UC—401
Unlimited Release
Printed August 1989

An Analysis of Solute Diffusion in the Culebra Dolomite

Ronald C. Dykhuizen, William H. Casey

Prepared by
Sandia National Laboratories
Albuquerque, New Mexico 87185 and Livermore, California 94550
for the United States Department of Energy
under Contract DE-AC04-76DP00789

Issued by Sandia National Laboratories, operated for the United States Department of Energy by Sandia Corporation.

Available to DOE and DOE contractors from
Office of Scientific and Technical Information
PO Box 62
Oak Ridge, TN 37831

Prices available from (615) 576-8401, FTS 626-8401

Available to the public from
National Technical Information Service
US Department of Commerce
5285 Port Royal Rd
Springfield, VA 22161

NTIS price codes
Printed copy: A03
Microfiche copy: A01

SAND--89-0750

DE90 000900

SAND89–0750
Unlimited Release
Printed August 1989

An Analysis of Solute Diffusion in the Culebra Dolomite

Ronald C. Dykhuizen
Fluid Mechanics & Heat Transfer Division III

William H. Casey
Geochemistry Division

Sandia National Laboratories
Albuquerque, NM 87185–5800

ABSTRACT

The diffusion of unreactive solutes through the Culebra Dolomite was studied experimentally and theoretically. The measured diffusive flux is less than that predicted from independent knowledge of the porosity and reasonable estimates of tortuosity. This low measured flux led to a review of the relationship between solute diffusion and pore geometry in rocks and sediments. Solute transport in hypothetical pore networks, where the effect of pore geometry on the solute flux is directly calculable, is examined. A conventional interpretation of pore tortuosity, as a normalized length of diffusion through a pore, loses meaning for cases where pores intersect in networks. Some important variables affecting the tortuosity are: (i) the distribution of pore sizes, (ii) the distribution of pore lengths, (iii) the number of pores which intersect at a node, and (iv) the pore shape between nodes. Furthermore, in porous materials with a preferential distribution of pore sizes and orientation, tortuosity is a tensor. For the Culebra Dolomite, the wide range of pore sizes causes the diffusive flux to vary considerably from that predicted from conventional theory. These results indicate that diffusive fluxes from fractures into rock pores may be smaller than previously thought.

1/2

Contents

Figures

SYMBOLS

A	area of the rock slab (cm^2)
A_{ij}	cross-sectional area of segment i in j
A_p	pore cross-sectional area (cm^2)
A'	pore area exposed parallel to the rock face (cm^2)
$C(t)$	concentration in the upper reservoir of the diffusion cell ($moles/cm^3$)
C_o	concentration of tracer in the lower reservoir ($moles/cm^3$)
ΔC_t	total change in concentration across the slab ($moles/cm^3$)
$\overline{\nabla} C$	solute concentration gradient ($moles/cm^4$)
D_e	$= \frac{\phi D^o}{\theta^2}$
D^o	the solute diffusion coefficient for an ion in solution $\left(\frac{cm^2}{s}\right)$
L_p	a pore length (cm)
J	solute flux normal to a rock slab ($moles/cm^2/s$)
$\overline{J}$	solute flux vector ($moles/cm^2/s$)
J_j	area-integrated solute flux across pore j ($moles/s$)
L	thickness of a rock slab (cm)
M	number of segments in a single pore
N	number of pores in a rock
V	volume of the upper reservoir of the diffusion cell
$f(x)$	probability density function (PDF) of property x;
g_{ij}	the conductance of segment i in pore j (cm^3/s) (7)
r	pore radius (cm^2)
t	time (s)
x_e	averaged (effective) value of x;
z	the connection number
ϕ	the rock porosity
θ	the average tortuosity of pores in the rock
ℓ	length of a pore segment (cm)
$\langle\rangle$	simply averaged quantities

1 INTRODUCTION

The need to predict rates of migration of toxic solutes from a buried waste repository to the biosphere has focused attention on models for water-rock interaction. Predictions are achieved by coupling models of solute transport to rate laws for reactions at mineral surfaces.

Difficulties arise in these models when solutes migrate through a fractured aquifer (*e.g.*, Neretniaks, 1980). Solutes are not only transported with groundwater in the connected fissures, but also diffuse into the adjacent rock pores. Thus rock pores temporarily store toxic solutes and, thereby, slow the rate of migration of these solutes to the biosphere. These diffusive fluxes arise in response to solute concentration gradients, such as those produced by diagenetic reactions in the rock pores, or by changing chemical conditions near the surface of the rock. Accurate estimation of diffusive fluxes into the rock from fractures is essential to understand the migration of toxic material in groundwater.

In many studies of solute diffusion in rocks, the flux is described with a simple equation (Bear, 1972):

$$\overline{J} = -D_e \overline{\nabla} C \quad , \tag{1}$$

where:

$$D_e = \frac{\phi \, D^o}{\theta^2} \quad .$$

In a standard treatment, the flux normal to a rock slab is calculated by considering the concentration gradient along any pore equal to the total difference in concentration across the rock, ΔC_t, divided by the rock thickness (L). This assumption amounts to considering the concentration field to be uniform in gradient across the sample:

$$J \approx -D_e \Delta C_t / L \quad . \tag{2}$$

The porosity and tortuosity terms which are implicit in Equations (1) and (2) account for the geometry of pores in a rock.

The treatment of solute diffusion via Equation (1) or (2) is appealing because the important parameters are easily estimated. Diffusion coefficients in solution are calculable (*e.g.*, Miller, 1982), and the total rock porosity is easily measured. Tortuosity

is estimated by comparing rates of solute transport through fluid-saturated rock with those rates in the fluid alone. These comparisons are often made conductometrically, which is direct and simple (*e.g.*, McDuff and Ellis, 1979). Furthermore, empirical relations exist to relate solute transport rates to porosity alone (*e.g.*, Ullman and Aller, 1982). With these empirical relations tortuosity can be completely eliminated from the transport equations.

Although these methods are commonly adequate, much can be learned by examining the theoretical relation of pore geometry and solute diffusion. The origin of the geometric terms in Equations (1) and (2) is often illustrated with the simple case of non-intersecting pores of constant area (*e.g.*, Ullman and Aller, 1982). In Figure 1, the fraction of the total rock area that consists of pores is given by the rock porosity ($\phi = A_p L_p / A_t L = A'/A_t$). Thus, in this simple example, porosity enters into the transport equations as a measure of the pore area exposed in a cross-section of rock.

Tortuosity is introduced as a scaling factor which accounts for the fact that pores are not oriented perpendicular to the rock face. In Figure 1, for example, the ratio of the true pore length to a straight pore is given by $\theta = L_p/L$. Tortuosity appears as a squared term in Equations (1) and (2) because the concentration gradient through the pore (Figure 1) is less than the macroscopic gradient and because the flux through the pore is oriented at some angle to slab normal. As we will show, this definition of tortuosity must be expanded for rocks which contain complicated pore networks.

We proceed in this examination in a stepwise manner. First, the diffusivity of samples of the Culebra Dolomite to unreactive solutes is measured. Then this diffusivity is compared to that predicted via Equation (1), using independent values of the rock porosity, and a tortuosity is obtained. This value of tortuosity tends to have little relationship to the classical interpretation of tortuosity (as described above), rather, it is used as a fitting parameter to account for the inadequacies of the model.

Secondly, we review the theoretical relation between pore geometry and solute diffusion. As part of this review, a hypothetical pore network is examined where the effect of pore geometry on solute diffusion can be calculated *a priori*. In these simulations tortuosity is calculated. With this more detailed model, tortuosity is returned to a physical basis.

We rely on the many experimental and theoretical studies of solute diffusion in rocks which precede this analysis (*e.g.*, Garrels, *et al.*, 1949; Brady, 1983; Norton and Knapp, 1977; Lever, *et al.*, 1985; Klinkenberg, 1951; many others). These studies are extended by introducing an important result from percolation theory (Kirkpatrick, 1973) which allows us to model solute diffusion in complicated pore networks (Benzoni and Chang, 1984; Burganos and Sortichos, 1987).

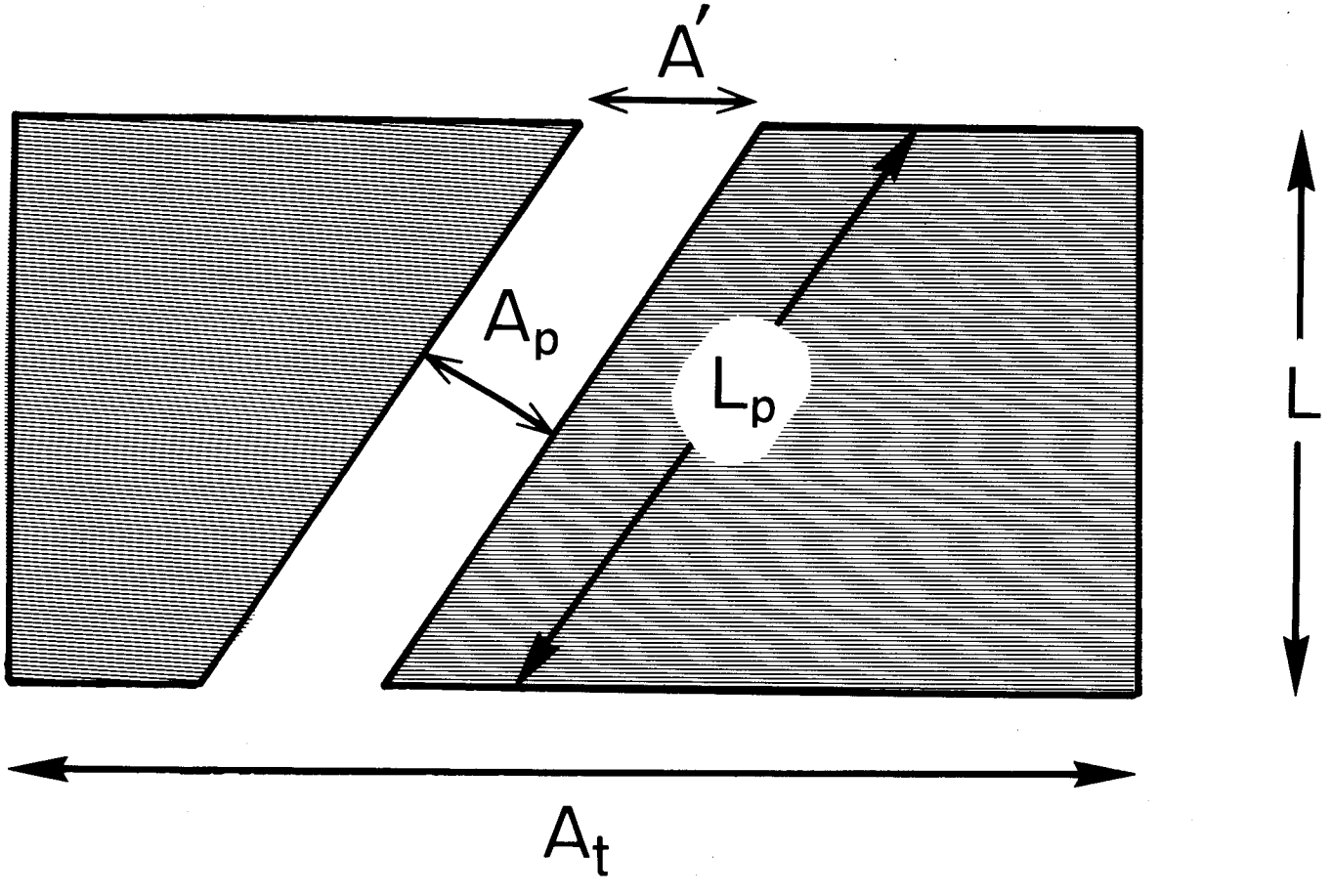

Figure 1. A pore geometry used to illustrate the relationship between diffusive flux and pore geometry (adapted from Ullmann and Aller, 1982).

2 EXPERIMENTAL METHODS

Unless otherwise noted, all uncertainties are reported as a single standard deviation, with n corresponding to the number of replicate analyses.

2.1 Description of the Culebra Dolomite

A rock sample of Culebra Dolomite was chosen for the experiment. The Culebra Dolomite is a subunit of the Rustler Formation of southwestern New Mexico (Adams, 1944). This unit overlies a proposed repository for radioactive waste (the Waste Isolation Pilot Plant) and is a locally important aquifer. The rock generally consists of fine-grained dolomite rhombs of about 1-10 microns in maximum dimension (see Figure 2), with lesser amounts of quartz, gypsum, halite, pyrite and clay. The material commonly contains small vugs ($\approx$ 1 mm diameter) where sulfate minerals have weathered out of the rock.

An experiment was conducted to measure the diffusivity of Culebra Dolomite to unreactive solutes. The diffusive properties of the Culebra Dolomite have been examined in several previous studies (Casey, *et al.*, 1987; Casey and Stockman, 1988a, Casey and Stockman, 1988b; Casey and Stockman, 1988c), which will be summarized further in this report. The purpose of this section is to familiarize the reader with methods of measuring rock diffusivities and to present a typical result. The experiment discussed in this section was performed on a fine-grained sample of Culebra Dolomite acquired from the 720 foot level during the shaft mapping project. The sample (ESM-143, 720') was taken by Robert Holt of the University of Texas at El Paso.

2.2 Porosity

Porosity was measured on subsamples of the rock using three separate techniques. Mercury porosimetry measurements were conducted by the Quantachrome Corporation at injection pressures of up to 60000 p.s.i. (see Lowell, 1979 for discussion of the method). The porosity measured in this fashion is 0.0730 ± 0.0037 ($n = 4$). Porosity measurements were also conducted on separate subsamples of rock by Terratek Laboratories using the Boyle' Law helium method (Coberly and Stevens, 1933). Using this method the porosity is 0.0975 ± 0.0024 ($n = 2$). Finally, the porosity was estimated by the water-loss method. In this method a sample of water-saturated rock of known volume is weighed, dried at 100°C, and reweighed. Porosity measured in this manner is 0.075 ± 0.0015 ($n = 2$).

It should not be surprising that these three techniques provide different estimates of rock porosity, as the methods are physically distinct from one another. Pores of $\approx$1

Figure 2. A backscattered electron photomicrograph of the Culebra Dolomite. This sample was used in the diffusion experiment and the scale bar is 100 micrometers.

Angstrom in nominal radius are accessible to helium, for example, but not to mercury, which is limited to rock pores greater than about 20 Angstroms in nominal radius (Lowell, 1979). Even with these differences, however, the porosity is reproducible to within a narrow range.

A vacuum technique was used to saturate pores in the rock with solution. The rock slab and plexiglas holder were placed in a vacuum chamber and repeatedly cycled between 150 and 760 torr. The sample was then immersed in solution, and both the solution and rock were repeatedly cycled in pressure. This treatment lasted a total of three days, after which the sample was placed in the diffusion cell with the background electrolyte solution.

2.3 The Diffusion Cell

The diffusion cell consists of two plexiglas reservoirs separated by a plexiglas plate containing a rock slab of known thickness and area (Figure 3). The rock slab is sealed into the plexiglas such that solutes diffuse between the two reservoirs through rock pores.

A tight seal between the rock core and plexiglas is achieved by coring the plexiglas to the same diameter as the rock sample. The core is then coated with a thin layer of epoxy and pressed into the plexiglas plate. The epoxy hardens and makes a tight seal between the rock core and the plexiglas. After the epoxy has dried, both the rock and plexiglas are ground to a uniform, flat surface. The integrity of the seal is tested by inducing a small pressure gradient across the rock slab, such that solution flows very slowly through the material. In all tests, fluid traveled through pores in the rock and not through the sealed edges. This criterion is used to infer that the sealed edges of the rock do not provide highly transmissive routes for solute migration.

During a typical experiment, each reservoir is filled with roughly 380 ml of brine solution. A small volume ($\approx$0.025 ml) of radioactive tracer is mixed into solution in the lower reservoir. The cell is then suspended from an overhead stirring apparatus so that the rock slab is horizontal (Figure 3) and immersed in an isothermal water bath (25°C). The entire cell is rotated discontinuously throughout the experiment to maintain well-mixed conditions in the cell. The mixing cycle consists of five seconds of rotation (36 r.p.m.) followed by five seconds of rest.

The upper reservoir is sampled at regular intervals by removing $\approx$1 ml of solution with a syringe. An equal volume of similar, although nonradioactive, solution is then added to the upper reservoir. Diffusion coefficients are calculated from the variation in concentration of the radioactive tracer with time in the upper reservoir.

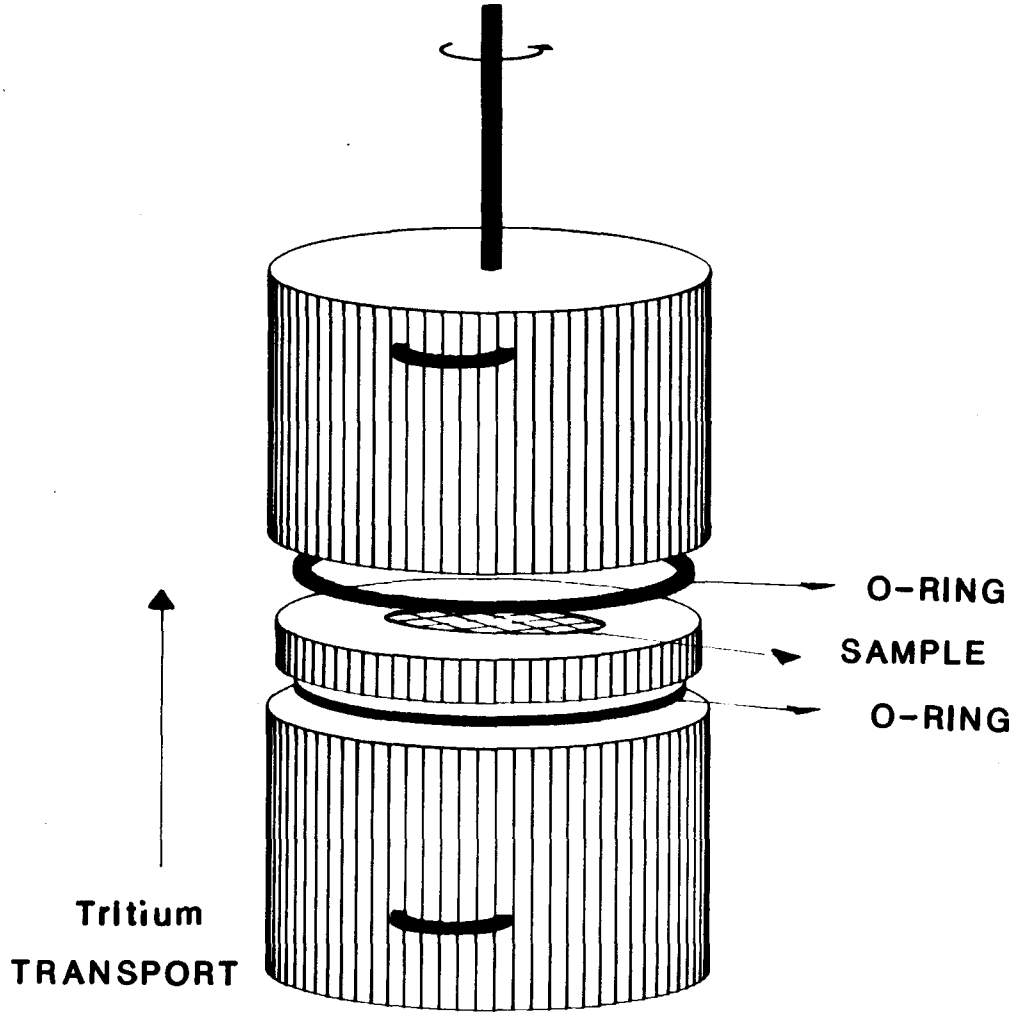

Figure 3. The diffusion cell.

2.4 Description of the Solution

The background electrolyte was chosen to minimize the dissolution or growth of minerals during the experiment. The solution was prepared by dissolving 700 g NaCl, 9.7 g $CaCl_2$, 12.5 g Na_2SO_4 and 0.026 g of $CaCO_3$ into two kilograms of tap water. This solution was then reacted with 10 g of finely ground rock for several days prior to each experiment, and had a final pH of approximately 6.9. This solution was then added to the diffusion cell and allowed to react further with the rock slab before adding the radioactive tracer. This period of pre-reaction allows the cell, rock and solution to approach chemical and thermal equilibrium prior to the experiment.

Tritium activity in the solution was measured by liquid scintillation counting using a cocktail appropriate for solutions of high ionic strength (Hionicfluor, Packard Instruments). The method was calibrated by counting standards of known activity in the experimental geometry. The precision is generally much better than 5%. Total activity of tritium was approximately 5 mCi.

2.5 Solute Transport Equation

The equations which describe solute transport in the cell, accepting the assumptions used in developing Equations (1) and (2), are well developed (Paul and DiBenedetto, 1965; Spacek and Kubin, 1967; Jenkins, *et al.*, 1969; Crank, 1975). As long as the concentration in the lower reservoir is approximately constant, and much larger than in the upper reservoir, the upper reservoir concentration is well described by an approximate solution. The concentration of radiotracer with time in the upper reservoir of the reaction cell is given by an equation of the form:

$$C(t) = \frac{\phi\ A_t\ L\ C_o}{V}\left[\frac{D^o t}{\theta^2\ L^2} - \frac{1}{6} + \frac{2}{\pi^2}\sum_{n=1}^{\infty}\frac{(-1)^n}{n^2}\exp\left(-\frac{D^o n^2\ \pi^2\ t}{\theta^2\ L^2}\right)\right] \quad . \qquad (3)$$

In this experiment, $L = 1.43(\pm 0.012)$ cm and $V = 381.1$ cm^3.

Equation (3) consists of a linear term and an exponential series. As time becomes large, the exponential term disappears asymptotically leaving a linear increase in concentration with time:

$$C(t) = \frac{\phi\ A_t\ L\ C_o}{V}\left[\frac{D^o\ t}{\theta^2\ L^2} - \frac{1}{6}\right] \quad . \qquad (4)$$

The time derivative of concentration, along with knowledge of the cell geometry, provides an estimate of the term $\frac{\phi D^o}{\theta^2}$ for the rock slab:

$$\frac{1}{C_o}\frac{dC}{dt} = \frac{\phi A_t D^o}{L V \theta^2} \quad . \tag{5}$$

Furthermore, the porosity of the sample is provided independently of the tortuosity from the intercept of Equation (4):

$$\frac{C(0)}{C_o} = \frac{-\phi A_t L}{6 V} \quad . \tag{6}$$

Thus both this porosity and the tortuosity can be determined from a single experiment. Using the simple model shown in Figure 1, this porosity corresponds to the exposed pore area in the sample. To avoid confusion in the upcoming section, we refer to this parameter as the diffusion porosity (Norton and Knapp, 1977). This diffusion porosity will be compared with the total rock porosity determined independently.

3 DISCUSSION OF THE EXPERIMENTAL RESULTS

Results of the experiment are shown in Figure 4. As predicted from the transport equations, tritium concentration increases linearly with time after a short interval in the early stages of the experiment. Also included in Figure 4 is a linear regression through the last 16 sample points. This regression slope is 5.9 ($\pm$ 0.04) 10^{-6} h^{-1} with an intercept of -8.1($\pm$0.3) 10^{-4}. These data can be used to estimate the tortuosity and pore area of the sample via Equations (5) and (6), provided that diffusion coefficients in solution can be estimated.

A tracer diffusion coefficient for tritium in 4.05 molar NaCl is provided by Devell (1962), who reports a value of 1.64($\pm$0.06) 10^{-5} cm^2/s. This value is adjusted to higher concentrations by correcting for viscosity (Harned and Owen, 1958), and thus we estimate a tracer diffusion coefficient of 1.31 10^{-5} cm^2/s for tritium under experimental conditions.

The diffusivity (D_e) and porosity of the rock are calculated to be 3.0($\pm$0.1) 10^{-8} cm^2/s and 0.04($\pm$0.005), respectively. The tortuosity (θ^2) is calculated to be 19. The diffusion porosity is considerably less than the porosity range measured via mercury, helium, or water porosimetry (0.075–0.0925). Therefore, our results indicate that the measured flux is much less than would be predicted from Equation (1) and independently measured porosities.

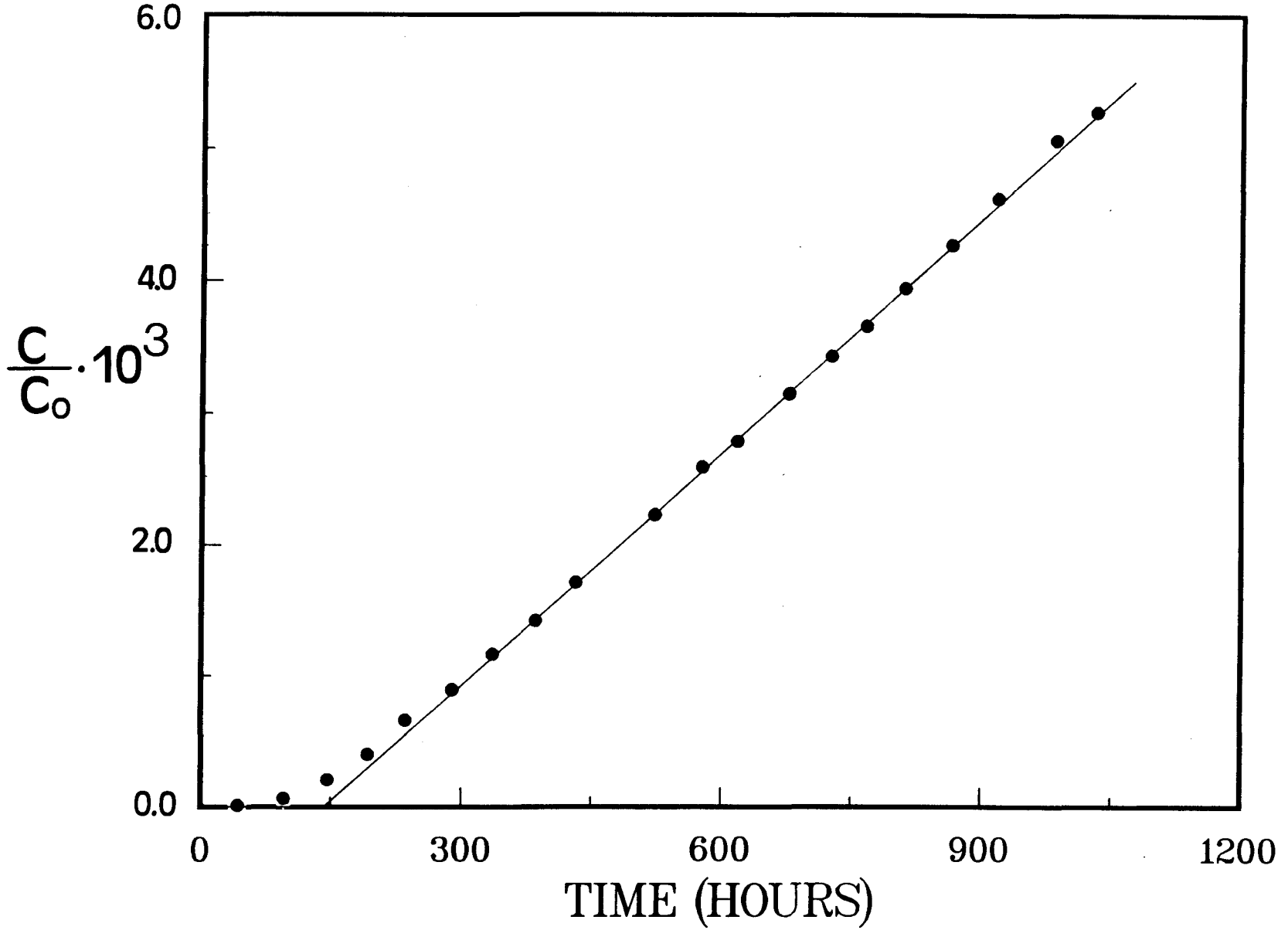

Figure 4. The reduced concentration of tritium in the upper portion of the diffusion cell as a function of time. Data are corrected for sampling, and the uncertainty due to counting statistics is contained within the sample point.

There are two potential causes of this low porosity. First, pores in the sample may not have been completely filled with solution prior to the experiment. Brace, *et al.*, (1965), for example, found that it was difficult to completely fill pores in granite with solution using techniques similar to those we employed here. The porosity of the granite (0.002–0.007), however, was roughly a factor of ten less than the Culebra Dolomite porosity (0.07–0.09) and, thus, may be more difficult to fill. Furthermore, the porosity determined by the water-loss method, which was determined after the diffusion experiments, is nearly equal to that measured via other methods.

A more likely cause of the low solute fluxes involves assumptions in the transport Equations (1), (2) and (3). These assumptions led us to review the relationship between pore geometry and solute diffusion.

4 SOLUTE DIFFUSION IN PORE NETWORKS

4.1 Porosity and Solute Diffusion

In real pore networks, pores vary in radius (and hence area) along their length. Solute diffusion through these pores varies considerably from the case of smooth-walled pores, such as those shown in Figure 1. These differences can be illustrated by examining two special cases.

In Figure 5 two sets of pores are shown arranged parallel to one another. No pores intersect and all are aligned normal to the rock slab, so that pore tortuosity defined via Figure 1 can be ignored. The pores are of equal length (L), and consist of smaller segments of equal length (ℓ). In Figure 5-A, pore segments of constant area are aligned to yield smooth sets of pores that completely traverse the rock. In Figure 5-B, pores consist of segments with varying area. The total rock porosities in Figures 5-A and 5-B are equal.

These two cases are chosen to resemble sets of electrical resistors arranged in parallel and in series. This similarity is maintained in our discussion by defining a conductance for each pore segment which is proportional to the segment area:

$$g_{ij} = \frac{A_{ij}\, D^o}{\ell} \quad \text{cm}^3/\text{s} \ , \tag{7}$$

where A_{ij} is the area of pore segment i in pore j. The total solute flux for each segment i in pore j is the same at steady state. Thus:

$$J_j = g_{ij} \Delta C_{ij} \quad \text{(moles/s)} \ , \tag{8}$$

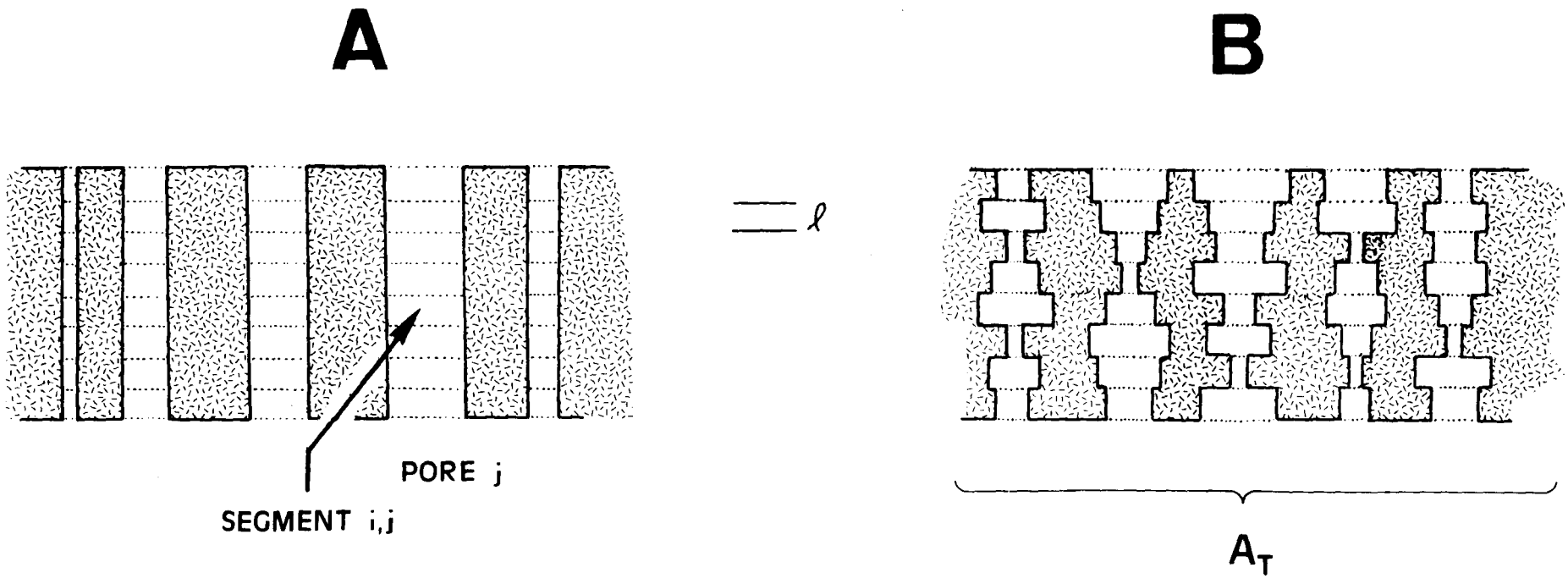

Figure 5. (A) The parallel model for arrangements of pore segments of length ℓ.
(B) The series model for arrangement of pore segments of length ℓ.

where ΔC_{ij} is the change in concentration across segment i in pore j (moles/cm^3).

The total change in concentration across the rock slab is found by summing over individual segments:

$$\Delta C_t = \sum_{i=1}^{M} \Delta C_{ij} = J_j \sum_{i=1}^{M} \frac{1}{g_{ij}} \quad \text{(moles/cm}^3\text{)} \ , \tag{9}$$

where M is the number of segments in the pore, which is equal to L/ℓ. Equation (9) is valid for all pores if the solution above and below the rock slab is well mixed.

With the above equations, differences between the two proposed pore geometries are shown in Figure 5. For the first case (Figure 5-A) the area of segments within a single pore is constant; thus $A_{ij} = A_{kj}$. Different pores, however, have different areas ($A_{ij} \neq A_{ik}$). There are N pores in the rock.

Therefore, Equation (9) may be simplified by noting that all conductances within a single pore are equal:

$$J_j = \frac{\Delta C_t \, g_{ij} \, \ell}{L} \quad \text{(moles/s)} \ . \tag{10}$$

By summing over all pores and dividing by the slab area, the flux through the rock is obtained:

$$J = \sum_{j=1}^{N} \frac{J_j}{A_t} = \frac{\Delta C_t \, \ell \, \sum_{j=1}^{N} g_{ij}}{L \, A_t} \quad \text{(moles/cm}^2\text{/s)} \ . \tag{11}$$

With a large number of pores, an average conductance can be used to replace the summation in Equation (11):

$$J = \frac{\Delta C_T \, \ell \, N \langle g_{ij} \rangle}{L \, A_t} \quad \text{(moles/cm}^2\text{/s)} \ . \tag{12}$$

Noting that the rock porosity can also be written in terms of the total number of pores:

$$\phi = \frac{N\langle A_{ij}\rangle}{A_t} \quad , \tag{13}$$

the flux through the rock is rewritten as:

$$J = \frac{\ell\ \phi\ \langle g_{ij}\rangle}{\langle A_{ij}\rangle}\ \frac{\Delta C_t}{L} \quad (\text{moles/cm}^2/\text{s}) \quad . \tag{14}$$

Note that Equation (14) resembles the flux defined in Equation (1), although it does not include a tortuosity term. (This resemblance becomes obvious when one uses Equation (7) to define the conductance.) Therefore, in the ensuing discussion Equation (1) is referred to as the parallel-pore model. This model of solute diffusion through pores is analogous to a parallel arrangement of electrical resistors.

The second case (Figure 5-B) yields a result similar to a series arrangement of electrical resistors. Again, the derivation begins with Equation (9), which is simplified by assuming that the number of segments in each pore is very large ($M >> 1$). In this case, the sum in Equation (9) can be replaced with M times the average value (recall $M = L/\ell$)

$$\Delta C_t = \frac{J_j\ L}{\ell}\ \langle\ \frac{1}{g_{ij}}\ \rangle \quad (\text{moles/cm}^3) \quad . \tag{15}$$

Note that each pore, j, contains many segments. Furthermore, if the segment areas are chosen from a single probability density function then the average term in Equation (15) is identical for all pores. That is, the average conductance of each pore is equal. In this case, the summation over all N pores can be replaced with N times the average flux through a single pore

$$J = \frac{\sum_{j=1}^{N}\ J_j}{A_T} = \frac{N\ \ell\ \Delta C_t}{A_T\ L\langle\frac{1}{g_{ij}}\rangle} \quad (\text{moles/cm}^2/\text{s}) \quad . \tag{16}$$

Again, introducing the porosity from Equation (13), the flux is rewritten as:

$$J = \frac{\ell\ \phi}{\langle A_{ij}\rangle L\langle\frac{1}{g_{ij}}\rangle}\frac{\Delta C_t}{L} \quad (\text{moles/cm}^2/\text{s}) \quad , \tag{17}$$

which is always smaller than the flux for the parallel case (except for the trivial case of monodisperse pores) since

$$\frac{1}{\langle \frac{1}{g_{ij}} \rangle} < \langle g_{ij} \rangle \quad . \tag{18}$$

Thus, the diffusivity of pore segments arranged in parallel is always larger than a series arrangement, even if the porosities are equal. In other words, the distribution of pore sizes in a rock strongly affects the observed flux.

The difference in fluxes for pores with constant and varying areas has been noted before (*e.g.*, Michaels, 1959; Petersen, 1955; van Brakel, *et al.*, 1974). These authors introduced an additional term (the constrictivity) to Equation (1) to reduce the calculated diffusivity from the parallel-pore model.

4.2 Tortuosity

The previous treatment can be easily adapted to include simple tortuosity, as illustrated in Figure 1, as long as only nonintersecting, parallel pores are considered. The treatment becomes very complicated, however, when pores intersect in complicated networks. Pore intersections change the functional dependence of solute flux on total porosity. Thus the tortuosity term assumes an additional meaning beyond that implied in the parallel-pore model (Figure 1).

Tortuosity is introduced when porosity (a volume term) is used to estimate a pore area available for diffusion. As illustrated in Figure 1, the actual porosity is an estimate of the area fraction of the rock surface which consists of exposed pores. This approximation is suitable in rocks which contain an isotropic and homogeneous pore network. As in the case of an inclined pore, however, the rock porosity must be corrected for the orientation of network pores.

Imagine a rock that contains the cubic pore network shown in Figure 6-A repeated *ad infinitem*. Two pore directions are exactly perpendicular to the macroscopic gradient in concentration. For this case, the entire flux proceeds by diffusion through pores parallel to the macroscopic gradient in concentration. Pores perpendicular to the concentration gradient contribute nothing to the net solute flux.

One interpretation of this special pore geometry is that the diffusion porosity should be set to $\frac{1}{3}$ the total porosity, since only $\frac{1}{3}$ of the pore volume contributes to the flux. Although this interpretation yields the correct flux, it is flawed. The interpretation leads to inaccurate prediction of the capacity of the rock to store solutes.

In this and the ensuing section, we show that there is no need for two separate porosities to model solute transport. The necessary correction factors can be calculated from pore geometry for some realistic cases.

Furthermore, the cubic grid shown in Figure 6-A is isotropic and yields the same solute flux regardless of the orientation of the macroscopic concentration gradient. For orientations where no pore set is exactly perpendicular to the concentration gradient, all of the pores will carry some flux, and the area fraction of pores on a plane perpendicular to the gradient will equal the rock porosity (not $\frac{1}{3}$ the porosity). Therefore, it appears that the diffusion porosity concept should be discarded. The actual rock porosity, along with a tortuosity term ($\theta^2 = 3.0$), more accurately represents the process of solute transport.

In this usage, tortuosity is a correction which accounts for orientation of pores relative to the concentration gradient and the rock surface. It is thus returned to the simple meaning implied by Figure 1. Both tortuosity and porosity can be related to physical properties of the rock. For those rocks which contain isotropic pore networks, the tortuosity is easily calculable (see Appendix).

Rock fabric introduces considerable uncertainty into the relationship between total porosity and diffusive flux. Consider the example shown in Figure 6-B where two sets of orthogonal pores of different diameters are shown. Because the solute flux is proportional to pore area, the diffusivity of the rock is largest parallel to the set of large pores. In the case shown in Figure 6-B, the set of small pores is parallel to the macroscopic concentration gradient. The large pores, and hence most of the rock porosity, contribute nothing to the flux. Total rock porosity is a particularly poor estimate of pore area in this case. We arbitrarily exclude pore intersections from this illustration to simplify the example. For the case shown in Figure 6-B, tortuosity is a tensor.

Even pore grids which are microscopically anisotropic, however, can be used to construct a much larger, isotropic pore network if they are repeated randomly in the rock. In this case, there is no preferred direction for solute migration through the rock. The equality $\theta^2 = 3.0$ again becomes true (Appendix). In Figure 6 only smooth, straight pores are considered. Curvature of the pore segments between intersections also complicates the treatment of tortuosity, but this effect is probably not large in most rocks.

A much larger effect is the presence of pore intersections and pores of varying area. Varying pore sizes in networks of intersecting pores introduces a resistance to diffusion in a manner similar to the one-dimensional arrangement of pores in series (Figure 5-B). When pores intersect, alternative paths exist around constricted segments. These alternative paths increase the macroscopic solute flux from the series example (Figure

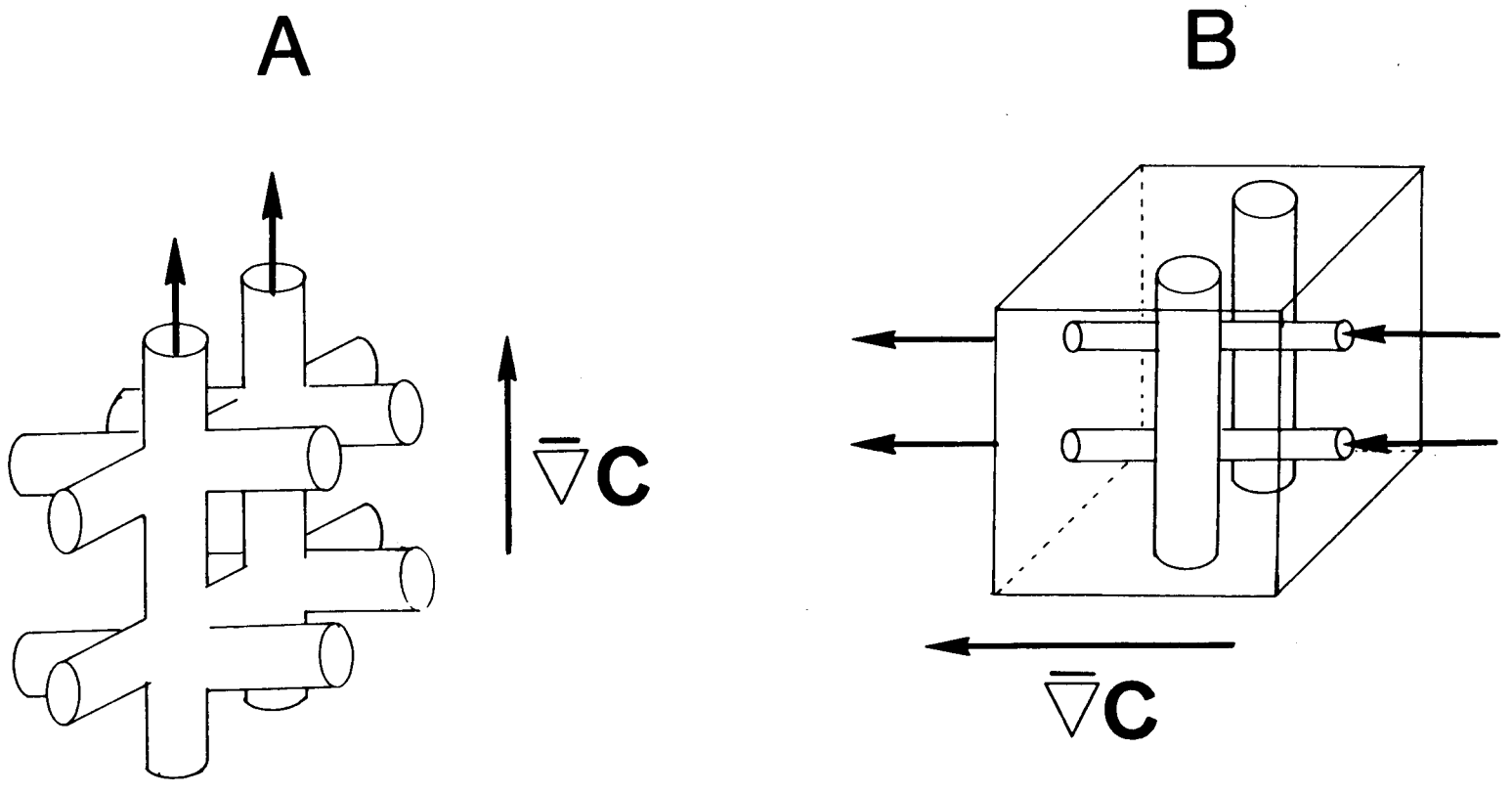

Figure 6. (A) An orthogonal network of uniform pores. (B) A network of non-uniform pores.

5-B), where solutes must diffuse through each pore constriction. The maximum flux is given by the parallel case (Figure 5-A), where there are no pore constrictions, and pores are straight.

Thus networks with varying pore radii have a flux which lies somewhere between the parallel and series examples shown in Figure 5. As we discuss in the next section, the degree to which the flux through a pore network resembles these limiting cases is affected by the distribution of pore radii and the geometry of the pore intersections.

5 MODELING SOLUTE TRANSPORT THROUGH THE CULEBRA DOLOMITE

To summarize, rock properties which affect the diffusive flux include: (i) the total porosity, (ii) the total variation and distribution of pore radii, (iii) rock fabric, and (vi) the degree to which pores deviate from a straight path between nodes. In addition, the character of intersections and the pore lengths between intersections affect the measured flux. These factors are all interrelated and their effects cannot be isolated in experiments on rocks.

However, the variables can be examined theoretically. In this section, solute transport is modeled through an idealized pore network where the effect of pore geometry on solute flux is directly calculable. Properties are assigned to this network which are similar to the Culebra Dolomite. Of the possible variables outlined above, the combined effects of pore intersections and pore constrictions on the solute flux are examined.

5.1 Effective Medium Theory

The construction of a model for rock pore network is illustrated in Figure 7. Although the depicted network is only two–dimensional, the calculations were performed for a three-dimensional network. In Figure 7-A a pore network is shown such as might be observed in the Culebra Dolomite. Pores are irregular in length, cross–sectional area and orientation. The treatment is simplified by postulating a network of straight pores of constant radius between intersections (Figure 7-B).

With detailed knowledge of pore areas, lengths, and orientations in the Culebra Dolomite, realistic properties could be assigned to the ideal network in Figure 7-B and a corresponding flux calculated. However, only the variation of pore radii is known for the Culebra Dolomite. Therefore, the network is idealized further, by postulating an isotropic grid of pores of constant length (Figure 7-C). The term θ^2 equals 3.0 for this grid, since the network is randomly oriented in space. This term would be slightly

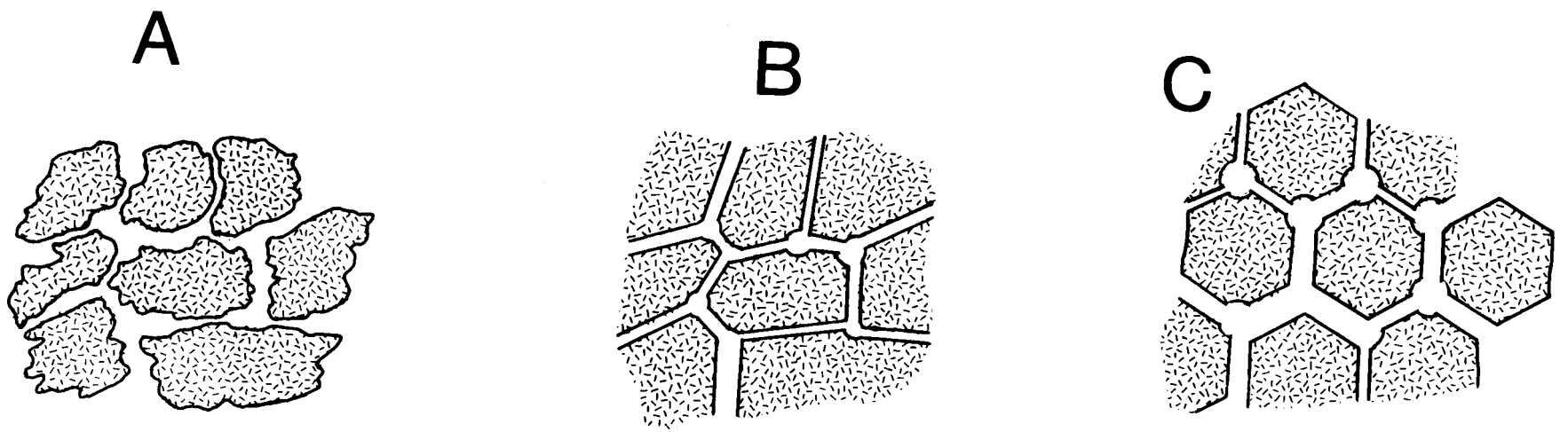

Figure 7. The modeling approach.

higher if pores are not smooth or straight between nodes. The results are independent of the pore length in this network.

Essential to these calculations is a method of averaging pore properties, so that the flux through each pore segment need not be treated individually. By analogy with networks of resistors, Kirkpatrick (1973), Benzoni and Chang (1984), and Burganos and Sotirchos (1987) provide a procedure to obtain an average conductance for a pore network such that the overall solute flux can be calculated. This averaging procedure recasts the pore network and yields an effective diffusivity that can be used in Equation (2).

The procedure to obtain an effective conductance greatly reduces the work needed to determine solute fluxes in pore networks. The averaging function is (Kirkpatrick, 1973):

$$\int \frac{(x_e - x)\, f(x)\, dx}{(z/2 - 1)\, x_e + x} = 0 \tag{19}$$

where $f(x)$ is the probability density function (PDF) of property x and x_e is the effective average value of x.

The connection number (z) is the number of pores leaving each node. For sake of comparison, the connection number of a cubic packing of spheres is six. A body-centered packing of spheres has a connection number of eight. Thus, there are valid reasons to suspect that the actual connection numbers of pores in a rock are small. Koplik, *et al.*, (1984), for example, measure a connection number of 3-4 for the Masillon sandstone by examining individual pores. Connection numbers less than two correspond to unconnected pores. Note that the averaging function includes only the connection number to describe pore topology; that is, cubic pore networks are equivalent to any other network with a connection number of 6.

From Equation (19), Burganos and Sotirchos (1987) calculated an effective diffusion coefficient for a medium consisting of cylindrical pores of constant length with radii selected from a known distribution, or:

$$D_e = \frac{\phi}{\theta^2}\, D^o \left[\frac{r^2}{\ell}\right]_e \frac{< \ell^2 >}{< r^2 \ell >} \quad . \tag{20}$$

Quantities in brackets, <>, are simply averaged. The subscript e indicates quantities averaged via Equation (19). The segment length in this case is between nodes in the network.

The accuracy was verified by comparing results from Equation (20) with Monte Carlo calculations of solute flux through an ideal rectangular pore network (Burganos and Sotirchos, 1987; see also Kirkpatrick, 1973). Benzoni and Chang (1984) also provide experimental verification for a pore network with bi-disperse sizes.

5.2 Application to the Culebra Dolomite

A pore-size distribution for the Culebra Dolomite is calculated from the relationship between mercury intrusion volume and pressure. Pore radii are calculated by assuming a cylindrical pore geometry and from knowledge of the surface tension of mercury (see Lowell, 1979). The integrated pore volume as a function of nominal pore radius is shown in Figure 8, along with a curve which was fit to the data for modeling purposes. The two curves are indistinguishable on the scale of the plot. The integrated pore volume at high pressure, of course, equals the total porosity of the rock ($\approx$0.07). The fitted curve was then differentiated with respect to pore number to produce a probability density function (Figure 9). This function was used to evaluate Equations (19) and (20).

Equation (20) was evaluated for connection numbers between 2 and 1000. Although connection numbers as high as 1000 are difficult to relate to rock properties, they have significance in terms of Equation (19) and are discussed below. Results of the calculations are shown in Figure 10.

In Figure 10 the ratio of the diffusion coefficient from the parallel-pore model (D_* in Equation (2)) to the effective diffusion coefficient (D_e) calculated with Equation (20) is shown. Tortuosity is equal in both cases ($\theta^2 = 3.0$). The essential difference between these two coefficients is that D_e includes the effect of pore constrictions and intersections on the solute flux.

As shown in Figure 10, the ratio varies from 1.0 at very large connection numbers, to approximately 0.1 at a connection number of 2. In other words, the standard approach to calculating diffusive fluxes (Equation (2)) becomes accurate as the number of pores leaving a node approaches infinity.

As discussed earlier, pore intersections cause the observed flux to be smaller than the parallel-pore model (Equation (2)), except for the trivial case of a network made up of uniform pore diameters. Equation (2) is least accurate for rocks with a wide distribution of pore sizes. For reasonable estimates of the connection number (two to ten) and the measured distribution of pore sizes in the Culebra Dolomite, diffusion coefficients calculated using Equation (2) are a factor of five too high. Burganos and Sotirchos (1987) show that the inaccuracy can be as large as a factor of ten for realistic pore-size distributions.

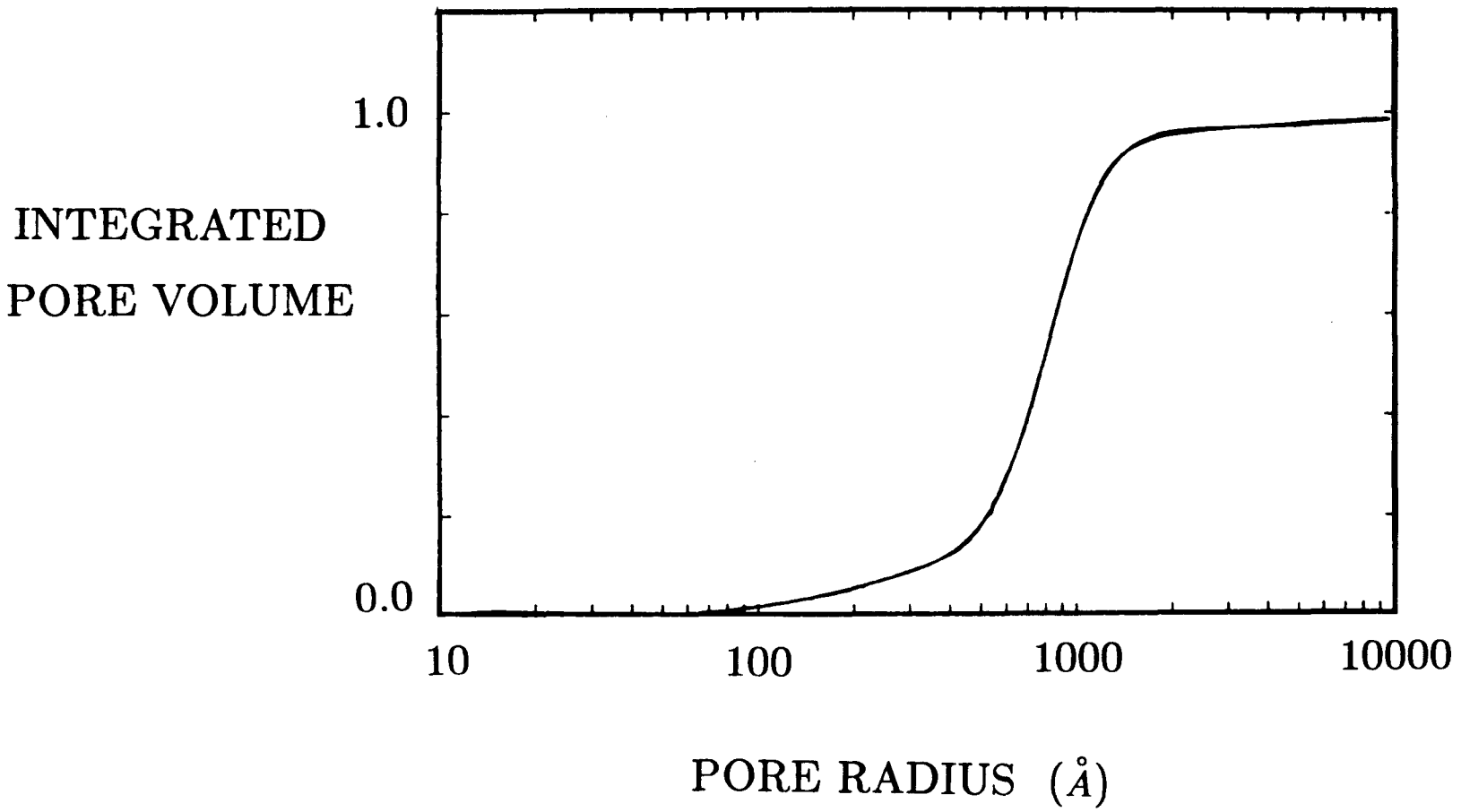

Figure 8. The integrated pore volume as a function of modeled pore radius.

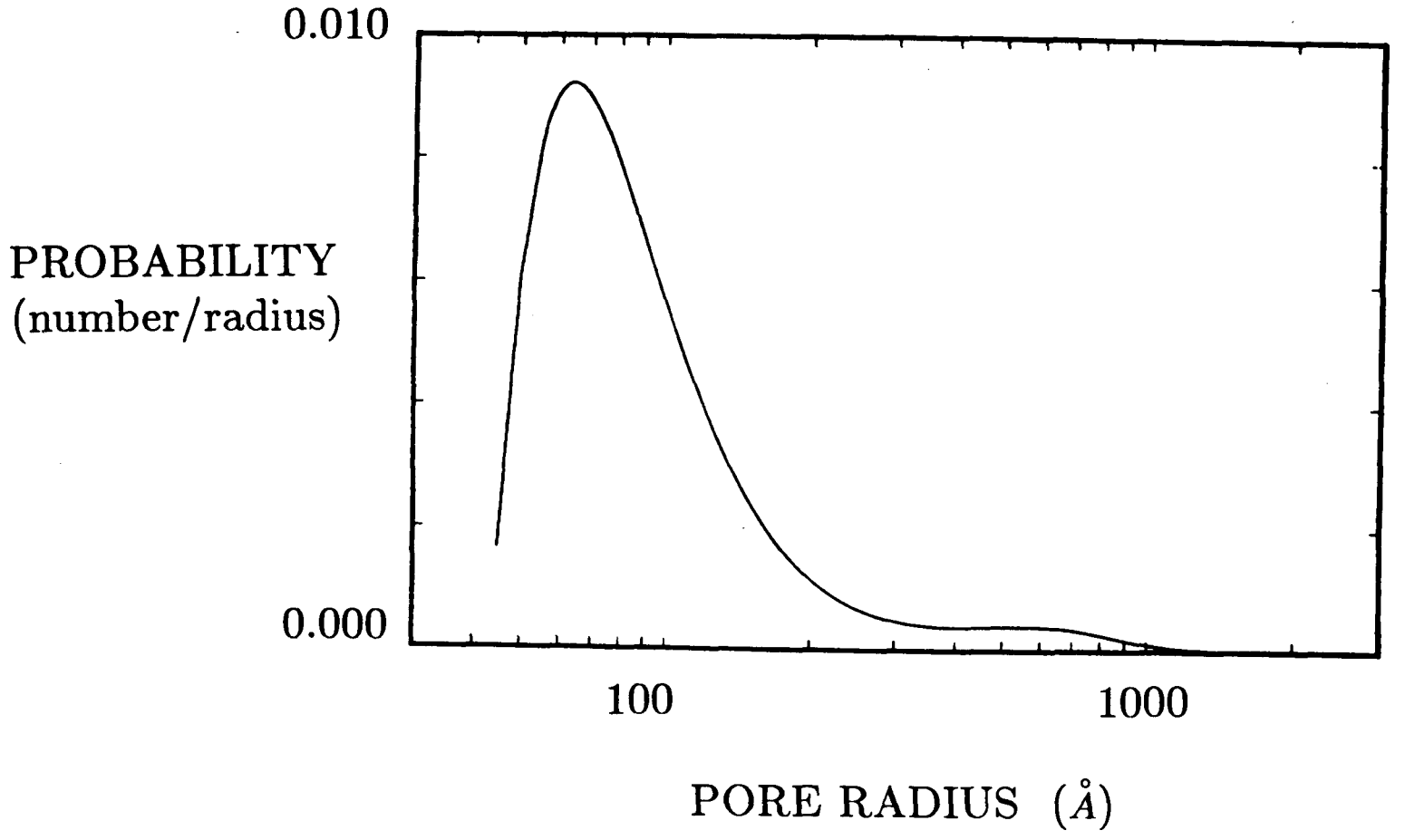

Figure 9. The probability density function (PDF) for pores in the Culebra Dolomite. The units are in number of pores per radius.

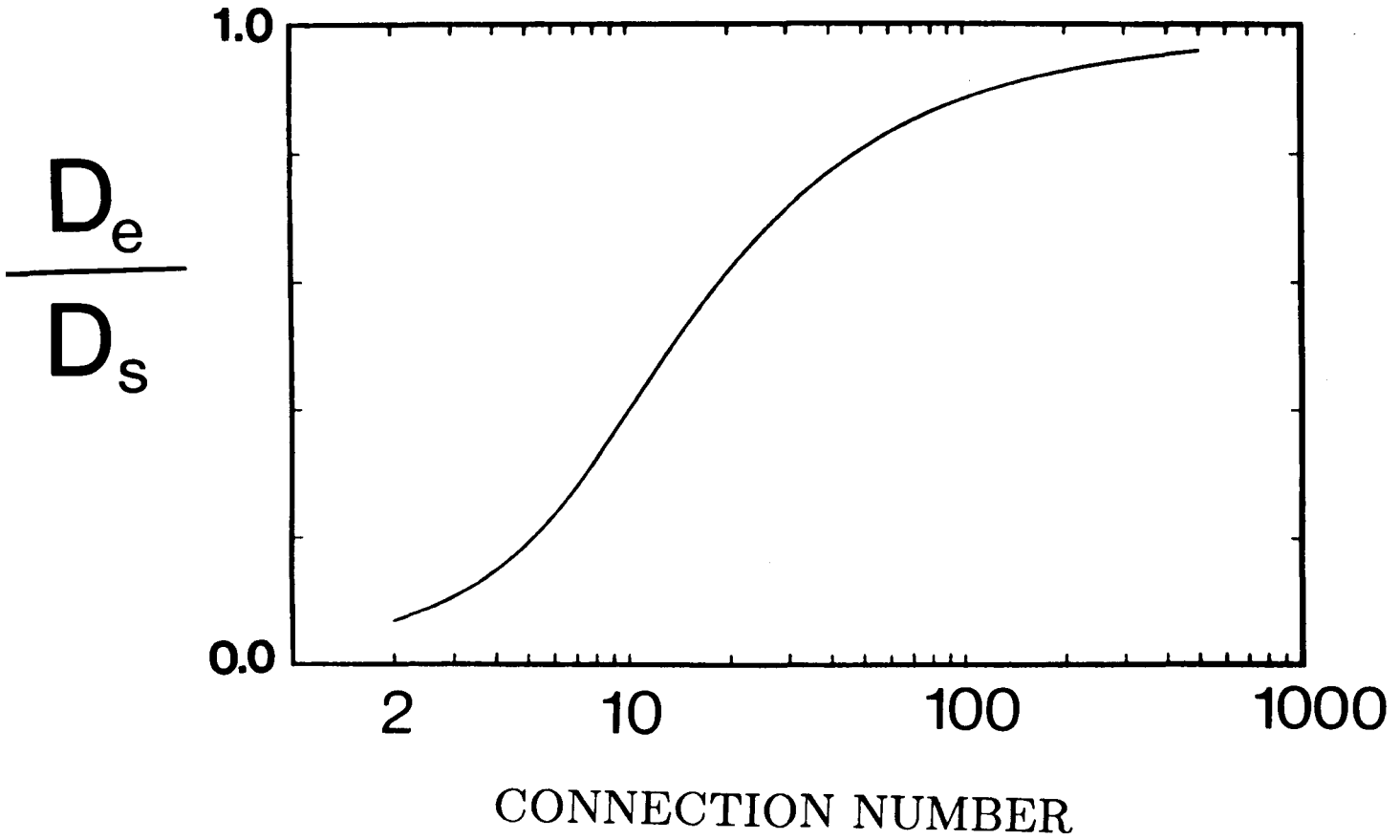

Figure 10. The variation in the ratio of the effective-medium diffusion coefficient to the parallel-model diffusion coefficient. In both cases, $\theta^2 = 3.0$.

A simple comparison can now be made of the pore network model presented here and the simple parallel-pore model of Equation (2). The diffusivity obtained experimentally for the Culebra Dolomite is $\approx 3 * 10^{-8}$ cm^2/s. From the experimental data, and Equations (1) through (3), this implies a diffusion porosity of 0.04 and $\theta^2 \approx 19$ or greater. We argue that these are essentially fitting parameters, since the diffusion porosity is half that measured by more accurate methods and the tortuosity is much higher than realistic models of pore structure.

The pore network theory also uses the functional form of Equation (2) to predict the diffusivity, but includes additional correction terms (Equation 20) which account for pore intersections and nonuniform pore sizes. When applying this model, the actual porosity of ≈ 0.08 is used, and θ^2 is set equal to 3.0. The same diffusion coefficient for tritium is used in both models. The correction terms to Equation (20) are obtained from Figure 10. For a connection number of 3, the correction terms yield a factor of $\approx$ 0.1. Thus we predict a diffusivity for the Culebra Dolomite of $3.5*10^{-8}$ cm^2/s, which is remarkably close to the experimental value given the level of approximation in the treatment.

This agreement is not entirely fortuitous. Our calculations are for an ideal pore network where the tortuosity is calculable ($\theta^2 = 3.0$), and with pore sizes similar to those measured on the sample of Culebra Dolomite. Thus, in our modeling, the measured distribution of pore sizes introduces a constrictivity to the isotropic grid. In this manner, we isolate some important geometric variables which affect solute diffusion in the Culebra Dolomite.

It is important to remember when interpreting Figure 10 that the calculations are for an ideal pore network where the tortuosity is calculable ($\theta^2 = 3.0$). Had this ideal pore network corresponded to an actual rock, the θ^2 term in Equation (2) would be measured to be larger than 3.0 to account for an anomalously low measured flux. That is, in practice, the tortuosity is an empirical scaling factor which relates solute flux to the measured porosity. The procedure outlined above returns tortuosity to a more physical interpretation.

At this point it is useful to review important assumptions in the model. We assume: (i) straight, smooth pores between nodes; (ii) a regular geometry of pores; (iii) pores of constant length; and (iv) random mixing of pore sizes from the PDFs shown in Figure 9. The results will, of course, change with different assumptions. In general, the parallel-pore model (Equation 2) becomes an accurate approximation to the true flux as: (i) the distribution of pore radii becomes unimodal with a small variance; and/or (ii) the number of pores intersecting at a node becomes large; or (iii) the pores resemble a smooth set of non-intersecting capillaries through the rock (the trivial case).

The use of the pore-size distribution shown in Figure 9 introduces a theoretical inconsistency into our treatment. The pore-size distribution was measured via mercury porosimetry, which employs an ideal model of the pore geometry (see Lowell, 1979). That is, the geometry assumed to calculate pore-size distributions from mercury intrusion is not the geometry used to evaluate Equation (20). This inconsistency is not critical, however, given other uncertainties in the calculation, but it can lead to low estimates of the actual number of large pores in the PDF (Wardlaw and Taylor, 1976).

The existence of dead-end pores is also not properly addressed in this model. Practically, dead-end pores can be included in the model by adding a finite number of pores with zero cross-sectional area. When these pores are distributed randomly in the pore network, they create pores with no net flux. The abundance of dead-end pores cannot be inferred from porosimetry data, and dead-end pores are, therefore, ignored in our treatment.

5.3 Summary of Other Results

The experiment discussed above is one of many which have been conducted on samples of the Culebra Dolomite. These results are reported in internal Sandia memoranda (Casey, *et al.*, 1987; Casey and Stockman, 1988a, 1988b, 1988c, Casey and Stockman, 1989). In these experiments, diffusion coefficients were calculated from the variation in activity with time of unreactive solute in the upper reservoir of the diffusion cell (*e.g.*, Figures 3 and 4). Regression parameters from the data are compiled in Table 1, along with standard estimates of the uncertainties. These regression data were used to calculate diffusivities using Equations (5) and (6).

The calculated transport properties are compiled in Table 2. Note that the diffusion porosity is generally less than the total porosity. The one exception is sample A1S-SNL-16, which has a highly uncertain estimate of diffusion porosity. The high uncertainty is attributable to the very small size of the sample (≈ 0.35 cm^3, Casey and Stockman, 1989).

An important conclusion from these experiments (Table 2) and the theoretical analysis presented above, is that the diffusive flux of solutes through the Culebra Dolomite cannot be estimated from knowledge of the total porosity. Many hydrologic models for solute migration through rock implicitly assume the parallel-pore model without actually measuring the diffusion porosity or tortuosity. This treatment commonly overestimates the diffusive flux and the retardation of solute by the formation. The inaccuracy depends upon the rock properties outlined above, as well as the technique for measuring the total rock porosity. Helium porosities, for example, are commonly much larger than the diffusion porosities. If rock contains a pronounced fabric,

Table 1. Regression Parameters

tracer	slope (H^{-1})	1σ	intercept	1σ	# points
		Sample ESM-143 720'			
Casey and Stockman (1988a)					
129_I	1.52*10^{-6}	4.63*10^{-8}	-1.63*10^{-4}	6.74*10^{-5}	15
22_{Na}	1.1*10^{-6}	4.3*10^{-8}	-1.5*10^{-4}	3.0*10^{-5}	16
Casey and Stockman (1988c)					
^{3}H	5.9*10^{-6}	4.3*10^{-8}	-8.1*10^{-4}	3.0*10^{-5}	16
		Sample Wipp-19 760.2'			
Casey and Stockman (1988b)					
^{22}Na	1.7*10^{-6}	9.3*10^{-8}	-8.7*10^{-4}	1.07*10^{-4}	6
^{3}H	4.1*10^{-6}	1.45*10^{-7}	-5.2*10^{-4}	1.2*10^{-4}	10
^{129}I	2.1*10^{-6}	3.4*10^{-8}	-2.1*10^{-4}	3.2*10^{-5}	21
^{22}Na	2.5*10^{-6}	8.3*10^{-8}	-5.3*10^{-4}	8.0*10^{-5}	13
		Sample A1S-SNL-16			
Casey and Stockman (1989)					
^{3}H	6.9*10^{-6}	0.04*10^{-6}	-1.9*10^{-5}	1.4*10^{-5}	15

Table 2: Transport Properties Calculated from the Diffusion of Solutes*

Tracer	$D = \frac{\phi D^o}{\theta^2}$ (cm^2/s)	Diffusion Porosity (ϕ)	Tortuosity (θ)	Total Porosity (ϕ)
		Sample ESM-143 720'		
Casey and Stockman (1988a)				0.072 – 0.098
^{129}I	$6.68 \pm 0.16*10^{-8}$	0.012 ± 0.003	3.37	
^{22}Na	$1.05 \pm 0.03*10^{-8}$	0.011 ± 0.002	3.28	
Casey and Stockman (1988c)				
^{3}H	$3.0 \pm 0.1*10^{-8}$	0.04 ± 0.005	5.5	
		Sample WIPP-19 760.2'		
Casey and Stockman (1988b)				0.086-0.155
^{22}Na	$1.3 \pm 0.14*10^{-8}$	0.04 ± 0.02	4.8	
^{3}H	$3.2 \pm 0.22*10^{-8}$	0.06 ± 0.02	6.3	
^{129}I	$1.6 \pm 0.05*10^{-8}$	0.02 ± 0.006	3.1	
^{22}Na	$1.9 \pm 0.06*10^{-8}$	0.04 ± 0.01	3.9	
		A1S-SNL-16		
Casey and Stockman (1989)				0.082 ± 0.002
^{3}H	$3.2 \pm 0.22*10^{-8}$	0.13 ± 0.34	1.9-2.4	

*Uncertainties are reported as two standard deviations. Total porosities were measured by mercury and helium porosimetry.

such as the case if fractures are lined by shale or claystone, the diffusivity is a tensor.

The measured diffusivity of Culebra Dolomite may be constrained with a series of simple conductance measurements in oriented samples (*e.g.*, McDuff and Ellis, 1979). The usefulness of these measurements, of course, depends upon the degree to which the rock samples are representative of the actual hydrology. There is, however, no reason to expect that field estimates of the rock diffusivity will be less uncertain than in these well-controlled experiments.

6 CONCLUSIONS

We have reviewed the relationship between pore geometry and solute diffusion in rocks. In this review, which was not comprehensive, we emphasized the following major points:

1. Rock porosity enters the transport equations as an estimate of the total fraction of pore area exposed in a random plane through the rock. This approximation is appropriate for homogeneous rocks with an isotropic pore network.
2. This total pore area is weighted by a constant of proportionality (tortuosity) to account for pores of differing orientations which contribute to the overall flux. For a homogeneous, isotropic pore network, $\theta^2 = 3.0$.
3. The distribution of pore sizes affects the flux by constricting the pathways of solute migration. In three-dimensional pore networks, intersections provide alternative pathways for solutes to migrate around constricted pore segments.

The importance of models which relate solute flux to actual rock properties cannot be overemphasized. A major obstacle to our understanding of diagenesis and metamorphism, for example, is our inability to estimate the exposed area of reactive minerals in a rock and the diffusive flux of solutes to this reactive area as a function of time. The first step toward correcting this inability is development and testing of models of the pore geometry.

These models are constructed by comparing measured diffusive fluxes of unreactive tracers with flux calculations on model pore networks. The comparisons are most useful when actual rock properties are assigned to the hypothetical network (*e.g.*, Koplik,, *et al.*, 1984). This approach was used to examine the diffusion of unreactive solutes through a sample of Culebra Dolomite. We find that the measured flux of solutes through the rock was more than a factor of two less than predicted from knowledge of the porosity and the measured tortuosity. This discrepancy disappears when a measured distribution of pore sizes is assigned to a hypothetical pore network.

7 ACKNOWLEDGEMENT

The authors would like to thank Steve Brown and Dave McTigue for important discussions about the modeling, and Harlan Stockman for help with solution analyses. Malcolm Siegel suggested a brine composition for these experiments based upon calculations from the program PREEQPTZ. Victoria McConnell helped with some of the illustrations and Henry Westrich produced the electron photomicrograph. This research was supported by the U.S. Department of Energy under contract DE-AC04-76DP00789.

8 REFERENCES

1. Adams, J. E. (1944). "Upper Permian Ochoa Series of Delaware Basin, West Texas and Southeastern New Mexico," Am. Assoc. Pet. Geol. Bull. 28, 1596-1625.

2. Bear, J. (1972). "Dynamics of fluids in Porous Media." American Elsevier, N.Y.

3. Benzoni, J. and Chang, H. C. (1984). "Effective Diffusion in Bidisperse Media: An Effective Medium Approach," Chem. Eng. Sci. 39, 163-165.

4. Berner, R. A. (1980). "Early Diagenesis: A Theoretical Approach," Princeton.

5. Brace, W. F.; Orange, A. S.; and Madden, T. R. (1965). "The Effect of Pressure on the Electrical Resistivity of Water-Saturated Crystalline Rocks," Jour. Geophys. Res. 70, 5669-5678.

6. Brady, J. B. (1983). "Intergranular Diffusion in Metamorphic Rocks," Amer. Jour. Sci. 283, 181-200.

7. Burganos, V. N. and Sotirchos, S. V. (1987). "Diffusion in Pore Networks: Effective Medium Theory and Smooth Field Approximation," AIChE Jour. 33, 1678-1689.

8. Casey, W. H.; Stockman, H. W.; Stein, C. L.; and Siegel, M. D. (1987). "Solute Diffusion Through Culebra Dolomite: Preliminary Experiments," unpublished memorandum to A. Lappin, November 21, 1988.

9. Casey, W. H. and Stockman, H. W. (1988a). Diffusion Porosities in Culebra Dolomite: Sample ESM-143," unpublished memorandum to A. Lappin, June 23, 1988.

10. Casey, W. H. and Stockman, H. W. (1988b). "Solute Diffusion Through Culebra Dolomite: Additional Results," unpublished memorandum to A. Lappin, March 23, 1988.

11. Casey, W. H. and Stockman, H. W. (1988c). "Low Diffusion Porosities in Culebra Dolomite," unpublished memorandum to A. Lappin, November 21, 1988.

12. Casey, W. H. and Stockman, H. W. (1989). "Solute Diffusion Through Sample A1S-SNL-16 of Culebra Dolomite," unpublished memorandum to A. Lappin, June 1, 1989.

13. Coberly, C. J. and Stevens, A. B. (1933). "Development of a Hydrogen Porosimeter," Oil Weekly 68, 9-22.

14. Crank, J., (1975). "The Mathematics of Diffusion," Oxford University Press, Oxford.

15. Devell, L. (1962). "Measurements of the Self-Diffusion of Water in Pure Water, H_2O-D_2O Mixtures and Solutions of Electrolytes," Acta Chemica Scand. 16, 2177-2188.

16. Garrels, R. M.; Dreyer, R. M.; and Howland A. L. (1949). "Diffusion of Ions Through Intergranular Spaces in Water-Saturated Rocks," Geol. Soc. Amer. Bull. 60, 1809-1828.

17. Harned, H. S. and Owen, B. B. (1958). "The Physical Chemistry of Electrolyte Solutions," Amer. Chem. Soc. Mono. 137. 803 pp.

18. Jenkins, R. C.; Nelson, P. M.; and Spirer, L. (1970). "Calculation of the Transient Diffusion of a Gas Through a Solid Membrane into a Finite Outflow Volume," Trans. Faraday Soc. 66, 1391-1401.

19. Kirkpatrick, S. (1973). "Percolation and Conduction," Rev. Mod. Physics 13, 574- 588.

20. Klinkenberg, L. J. (1951). "Analogy Between Diffusion and Electrical Conductivity in Porous Rocks," Geol. Soc. Amer. Bull., 62, 559-564.

21. Koplik, J.; Lin, C.; and Vermette, M. (1984). "Conductivity and Permeability from Microgeometry," Jour. Appl. Phys. 56, 3127-3131.

22. Krom, M. D. and Berner, R. A. (1980). "The Experimental Determination of the Diffusion Coefficients of Sulfate, Ammonium, and Phosphate in Anoxic Marine Sediments," Limnol. and Oceanog. 25, 327-337.

23. Lever, D. A.; Bradbury, M. H.; and Hemingway, S. J. (1985). "The Effect of Dead-End Porosity on Rock-Matrix Diffusion," Jour. Hydrol. 80, 45-76.

24. Lowell, S. (1979). "Introduction to Powder Surface Area," Wiley-Interscience. 197 pp.

25. McDuff, R. E. and Ellis, R. A. (1979). "Determining Diffusion Coefficients in Marine Sediments: A Laboratory Study of the Validity of Resistivity Techniques," Amer. Jour. Sci. 279, 666-675.

26. Michaels, A. S. (1959). "Diffusion in a Pore of Irregular Geometry–A Simplified Treatment," Amer. Inst. Chem. Eng. Journal 5, 270-271.

27. Miller, D. G. (1982). "Estimation of Tracer Diffusion Coefficients of Ions in Aqueous Solutions," Report UCRL-53319, Lawrence Livermore National Laboratory, 17pp.

28. Norton, D. and Knapp, R. (1977). "Transport Phenomena in Hydrothermal Systems: The Nature of Porosity," Amer. Jour. Sci., 277, 913-936.

29. Paul, D. R. and DiBenedetto, A. T. (1965). "Diffusion in Amorphous Polymers," Jour. Polymer. Sci. C, 17-44.

30. Petersen, E. E. (1955). "Diffusion in a Pore of Varying Cross Section," Amer. Inst. Chem. Eng. Jour. 4, 343-345.

31. Spacek, P. and Kubin, M. (1967). "Diffusion in Gels," Jour. Polym. Sci. C, 705–714.

32. Turk, J. T. (1976). "A Study of Diffusion in Clay-Water Systems by Chemical and Electrical Methods," unpub. Ph.D thesis, Univ. of California, San Diego, 111 p.

33. Ullman, W. J. and Aller, R. C. (1982). "Diffusion Coefficients in Nearshore Marine Sediments," Limnol. Oceanogr. 27, 552-556.

34. van Brakel, J. and Heertjes, P. M. (1974). "Analysis of Diffusion in Terms of a Porosity, a Tortuosity and a Constrictivity Factor," Int. J. Heat Mass Transfer 17, 1093-95.

35. Wardlaw, N. C. and Taylor, R. P. (1976). "Mercury Capillary Pressure Curves and the Interpretation of Pore Structure and Capillary Behavior in Reservoir Rocks," Bull. Can. Petrol. Geol. 17, 225-262.

Appendix

Buragnos and Sotirchos (1987) state that θ^2 is equal to the inverse of the dimensionality for an isotropic network, such as the cubic network shown in Figure 6-A. Other pore grids may also be isotropic if they are oriented randomly throughout the rock.

Proof is derived from the inclined–pore model for tortuosity (Figure 1) and the assumption that all pore orientations are equally likely. If we employ standard spherical coordinates to represent three-dimensional space, an integral average can be performed to obtain the tortuosity:

$$\frac{1}{\theta^2} = < \left[\frac{L}{L_P}\right]^2 > \tag{21}$$

$$= \frac{\int_o^{2\pi} \int_o^{\pi/2} \left[\frac{L_P \cos\psi}{L_P}\right]^2 \sin\psi \, d\psi \, d\zeta}{\int_o^{2\pi} \int_o^{\pi/2} \sin\psi \, d\psi \, d\zeta} = \frac{1}{3} \tag{22}$$

In Equation (1), we use ψ and ζ to represent the azimuthal and polar angles of the sphere of integration.

Distribution:

U. S. Department of Energy, (5)
Office of Civilian Radioactive Waste
Management
Attn: Deputy Director, RW-2
Associate Director, RW-10
Office of Program Administration
and Resources Management
Associate Director, RW-20
Office of Facilities Siting
and Development
Associate Director, RW-30
Office of Systems Integration
and Regulations
Associate Director, RW-40
Office of External Relations
and Policy
Forrestal Building
Washington, DC 20585

U. S. Department of Energy (3)
Albuquerque Operations Office
Attn: Bruce G. Twining
J. E. Bickel
R. Marquez, Director
Public Affairs Division
P.O. Box 5400
Albuquerque, NM 87185

U. S. Department of Energy
Attn: National Atomic Museum Library
Albuquerque Operations Office
P. O. Box 5400
Albuquerque, NM 87185

U. S. Department of Energy (9)
WIPP Project Office (Carlsbad)
Attn: J. Tillman (4)
A. Hunt
T. Lukow (2)
V. Daub
B. Young
P.O. Box 3090
Carlsbad, NM 88221

U. S. Department of Energy
Research & Waste Management Division
Attn: W. R. Bibb, Director
P. O. Box E
Oak Ridge, TN 37831

U.S. Department of Energy
Richland Operations Office
Nuclear Fuel Cycle & Production
Division
Attn: R. E. Gerton
P.O. Box 500
Richland, WA 99352

U. S. Department of Energy (5)
Office of Defense Waste and
Transportation Management
Attn: T. B. Hindman----- DP-12
M. Duff --------- DP-123
A. Follett ------- DP-122
C. H. George ----- DP-124
J. Mathur -------- DP-123
Washington, DC 20545

U. S. Department of Energy (2)
Idaho Operations Office
Fuel Processing and Waste
Management Division
785 DOE Place
Idaho Falls, ID 83402

U.S. Department of Energy (3)
Savannah River Operations Office
Defense Waste Processing
Facility Project Office
Attn: S. Cowan
W. J. Brumley
P.O. Box A
Aiken, SC 29802

U.S. Environmental Protection Agency
Attn: D. J. Egan, Jr.
Mark Cotton
Office of Radiation Programs (ANR-460)
Washington, DC 20460

U.S. Geological Survey
Branch of Regional Geology
Attn: R. Snyder
MS913, Box 25046
Denver Federal Center
Denver, CO 80225

U.S. Geological Survey
Conservation Division
Attn: W. Melton
P.O. Box 1857
Roswell, NM 88201

U.S. Geological Survey (2)
Water Resources Division
Attn: Cathy Peters
Suite 200
4501 Indian School, NE
Albuquerque, NM 87110

U.S. Nuclear Regulatory Commission (4)
Division of Waste Management
Attn: Michael Bell
Hubart Miller
Jacob Philip
NRC Library
Mail Stop 623SS
Washington, DC 20555

Environmental Evaluation Group (3)
Attn: Library
Suite F-2
7007 Wyoming Blvd., N.E.
Albuquerque, NM 87109

New Mexico Bureau of Mines
and Mineral Resources (2)
Attn: F. E. Kottolowski, Director
J. Hawley
Socorro, NM 87801

NM Department of Energy & Minerals
Attn: Kasey LaPlante, Librarian
P.O. Box 2770
Santa Fe, NM 87501

Battelle Pacific Northwest Laboratories (6)
Attn: D. J. Bradley
J. Relyea
R. E. Westerman
S. Bates
H. C. Burkholder
L. Pederson
Battelle Boulevard
Richland, WA 99352

Savannah River Laboratory (6)
Attn: N. Bibler
E. L. Albenisius
M. J. Plodinec
G. G. Wicks
C. Jantzen
J. A. Stone
Aiken, SC 29801

Savannah River Plant
Attn: Richard G. Baxter
Building 704-S
Aiken, SC 29808

George Dymmel
SAIC
101 Convention Center Dr.
Las Vegas, NV 89109

INTERA Technologies, Inc. (4)
Attn: G. E. Grisak
J. F. Pickens
A. Haug
A. M. LeVenue
Suite #300
6850 Austin Center Blvd.
Austin, TX 78731

INTERA Technologies, Inc.
Attn: Wayne Stensrud
P.O. Box 2123
Carlsbad, NM 88221

IT Corporation (2)
Attn: R. F. McKinney
J. Myers
Regional Office - Suite 700
5301 Central Avenue, NE
Albuquerque, NM 87108

IT Corporation (2)
Attn: D. E. Deal
P.O. Box 2078
Carlsbad, NM 88221

Charles R. Hadlock
Arthur D. Little, Inc.
Acorn Park
Cambridge, MA 02140-2390

Los Alamos Scientific Laboratory
Attn: B. Erdal, CNC-11
Los Alamos, NM 87545

Oak Ridge National Laboratory (4)
Attn: R. E. Blanko
E. Bondietti
C. Claiborne
G. H. Jenks
Box Y
Oak Ridge, TN 37830

RE/SPEC, Inc.
Attn: W. Coons
P. F. Gnirk
P.O. Box 14984
Albuquerque NM 87191

RE/SPEC, Inc. (7)
Attn: L. L. Van Sambeek
D. B. Blankenship
G. Callahan
T. Pfeifle
J. L. Ratigan
P. O. Box 725
Rapid City, SD 57709

Rockwell International (1)
Attn: C. E. Wickland
Rocky Flats Plant
Golden, CO 80401

Rockwell International (3)
Atomics International Division
Rockwell Hanford Operations
Attn: J. Nelson (HWVP)
P. Salter
W. W. Schultz
P.O. Box 800
Richland, WA 99352

Science Applications
International Corporation
Attn: Howard R. Pratt,
Senior Vice President
10260 Campus Point Drive
San Diego, CA 92121

Science Applications
International Corporation
Attn: Michael B. Gross
Ass't. Vice President
Suite 1250
160 Spear Street
San Francisco, CA 94105

Systems, Science, and Software (2)
Attn: E. Peterson
P. Lagus
Box 1620
La Jolla, CA 92038

Westinghouse Electric Corporation (7)
Attn: Library
W. C. Moffitt
W. P. Poirer
W. R. Chiquelin
V. F.Likar
D. J. Moak
R. F. Kehrman
P. O. Box 2078
Carlsbad, NM 88221

T. N. Narasimhan
Earth Sciences Division
Lawrence Berkeley Laboratory
University of California
Berkeley, CA 94720

University of Arizona
Attn: J. G. McCray
Department of Nuclear Engineering
Tucson, AZ 85721

University of New Mexico (2)
Geology Department
Attn: D. G. Brookins
Library
Albuquerque, NM 87131

Pennsylvania State University (1)
Materials Research Laboratory
Attn: Della Roy
University Park, PA 16802

Texas A&M University
Center of Tectonophysics
College Station, TX 77840

G. Ross Heath
College of Ocean
and Fishery Sciences
University of Washington
Seattle, WA 98195

Thomas Brannigan Library
Attn: Don Dresp, Head Librarian
106 W. Hadley St.
Las Cruces, NM 88001

Hobbs Public Library
Attn: Ms. Marcia Lewis, Librarian
509 N. Ship Street
Hobbs, NM 88248

New Mexico State Library
Attn: Ms. Ingrid Vollenhofer
P.O. Box 1629
Santa Fe, NM 87503

New Mexico Tech
Martin Speere Memorial Library
Campus Street
Socorro, NM 87810

Pannell Library
Attn: Ms. Ruth Hill
New Mexico Junior College
Lovington Highway
Hobbs, NM 88240

WIPP Public Reading Room
Attn: Lee Hubbard, Head Librarian
Carlsbad Municipal Library
101 S. Halagueno St.
Carlsbad, NM 88220

Government Publications Department
General Library
University of New Mexico
Albuquerque, NM 87131

Dr. Charles Fairhurst, Chairman
Department of Civil and
Mineral Engineering
University of Minnesota
500 Pillsbury Dr. SE
Minneapolis, MN 55455

Dr. John O. Blomeke
Route 3
Sandy Shore Drive
Lenoir City, TN 37771

Dr. John D. Bredehoeft
Western Region Hydrologist
Water Resources Division
U.S. Geological Survey (M/S 439)
345 Middlefield Road
Menlo Park, CA 94025

Dr. Karl P. Cohen
928 N. California Avenue
Palo Alto, CA 94303

Dr. Fred M. Ernsberger
250 Old Mill Road
Pittsburgh, PA 15238

Dr. Rodney C. Ewing
Department of Geology
University of New Mexico
200 Yale, NE
Albuquerque, NM 87131

Dr. George M. Hornberger
Department of Environmental Sciences
Clark Hall
University of Virginia
Charlottesville, VA 22903

Dr. Frank L. Parker
Department of Environmental
Engineering
Vanderbilt University
Nashville, TN 37235

Dr. D'Arcy A. Shock
233 Virginia
Ponca City, OK 74601

Dr. Christopher G. Whipple
Electric Power Research Institute
3412 Hillview Avenue
Palo Alto, CA 94303

Dr. Peter B. Myers, Staff
Director
National Academy of Sciences
Committee on Radioactive
Waste Management
2101 Constitution Avenue
Washington, DC 20418

Ina Alterman
Board on Radioactive Waste
Management
GF462
2101 Constitution Avenue
Washington, D. C. 20418

Studiecentrum Voor Kernenergie (1)
Centre D'Energie Nucleaire
Attn: Mr. A. Bonne
SCK/CEN
Boeretang 200
B-2400 Mol
BELGIUM

Atomic Energy of Canada, Ltd. (2)
Whiteshell Research Estab.
Attn: Peter Haywood
John Tait
Pinewa, Manitoba, CANADA
ROE 1L0

Dr. D. K. Mukerjee
Ontario Hydro Research Lab
800 Kipling Avenue
Toronto, Ontario, CANADA
M8Z 5S4

Mr. D. Alexandre, Deputy Director
ANDRA
31, Rue de la Federation
75015 Paris, FRANCE

Mr. Jean-Pierre Olivier
OECD Nuclear Energy Agency
Division of Radiation Protection
and Waste Management
38, Boulevard Suchet
75016 Paris, FRANCE

Claude Sombret
Centre D'Etudes Nucleaires
De La Vallee Rhone
CEN/VALRHO
S.D.H.A. BP 171
30205 Bagnols-Sur-Ceze
FRANCE

Bundesministerium fur Forschung und
Technologie
Postfach 200 706
5300 Bonn 2
FEDERAL REPUBLIC OF GERMANY

Bundesanstalt fur Geowissenschaften
und Rohstoffe
Attn: Michael Langer
Postfach 510 153
3000 Hannover 51
FEDERAL REPUBLIC OF GERMANY
Hahn-Mietner-Institut fur Kernforschung (1)
Attn: Werner Lutze
Glienicker Strasse 100
100 Berlin 39
FEDERAL REPUBLIC OF GERMANY

Institut fur Tieflagerung (4)
Attn: K. Kuhn
Theodor-Heuss-Strasse 4
D-3300 Braunschweig
FEDERAL REPUPLIC OF GERMANY

Kernforschug Karlsruhe (1)
Attn: K. D. Closs
Postfach 3640
7500 Karlsruhe
FEDERAL REPUBLIC OF GERMANY

Physikalisch-Technische Bundesanstalt
Attn: Peter Brenneke
Postfach 33 45
D-3300 Braunschweig
FEDERAL REPUBLIC OF GERMANY

D. R. Knowles
British Nuclear Fuels, plc
Risley, Warrington, Cheshire WA3 6AS
1002607 GREAT BRITAIN

Shingo Tashiro
Japan Atomic Energy Research Institute
Tokai-Mura, Ibaraki-Ken
319-11 JAPAN

Netherlands Energy Research Foundation
ECN (2)
Attn: Tuen Deboer, Mgr.
L. H. Vons
3 Westerduinweg
P.O. Box 1
1755 ZG Petten, THE NETHERLANDS

Svensk Karnbransleforsorjning AB
Attn: Fred Karlsson
Project KBS
Karnbranslesakerhet
Box 5864
10248 Stockholm, SWEDEN

Sandia Internal:

1510 J. W. Nunziato
1511 D. K. Gartling
1511 R. R. Eaton
1511 P. L. Hopkins
1511 M. J. Martinez
1511 D. F. Mctigue
1512 J. C. Cummings
1512 K. L. Erickson
1513 D. W. Larson
1513 R. C. Dykhuizen (10)
1520 L. W. Davison
1521 R. D. Krieg
1521 J. G. Arguello
1521 H. S. Morgan
1530 D. B. Hayes
1550 C. W. Peterson
3141 S. A. Landenberger (5)
3151 W. I. Klein (3)
3154-1 C. L. Ward, (8) for DOE/OSTI
6000 D. L. Hartley
6230 W. C. Luth
6231 H. C. Hardee
6232 W. R. Wawersik
6233 T. M. Gerlach
6233 W. H. Casey (10)
6233 J. L. Krumhansl
6233 H. W. Stockman
6233 M. E. Thompson
6300 R. W. Lynch
6310 T. O. Hunter
6312 P. A. Kaplan
6312 M. S. Tierney
6312 M. L. Wilson
6313 T. Blejwas
6315 L. E. Shephard
6315 R. J. Glass
6330 W. D. Weart
6330 V. L. Bruch
6330 D. P. Garber
6330 S. Pickering
6331 A. R. Lappin
6331 R. L. Beauheim
6331 D. J. Borns
6331 P. B. Davies
6331 S. J. Lambert
6331 R. Z. Lawson
6331 K. L. Robinson

6331 M. D. Siegel
6332 L. D. Tyler
6332 R. Beraun
6332 B. M. Butcher
6332 B. L. Ehgartner
6332 S. J. Finley
6332 M. A. Molecke
6332 D. E. Munson
6332 E. J. Nowak
6332 J. C. Stormont
6332 T. M. Torres
6332 Sandia WIPP Central Files (10)
6333 T. M. Schultheis
6334 D. R. Anderson
6334 G. T. Barker
6334 S. Bertram-Howery
6334 K. Brinster
6334 L. Brush
6334 G. E. Bujewski
6334 L. S. Gomez
6334 R. Guzowski
6334 R. L. Hunter
6334 M. G. Marietta
6334 R. R. Rechard
6334 A. Rutledge
6410 N. R. Ortiz
6416 E. J. Bonano
7100 C. D. Broyles
7110 J. D. Plimpton
7120 M. J. Navratil
7125 R. L. Rutter
7125 J. T. McIlmoyle
7130 J. O. Kennedy
7133 O. Burchett
7133 J. W. Mercer
7135 P. D. Seward
8524 J. A. Wackerly (SNLL Library)